

Electronic Supplementary Information

A polysaccharide matrix for the storage and controlled release of reagents in inkjet-printed point-of-care cell counting chambers

Xichen Zhang^a, Dorothee Wasserberg^a, Christian Breukers^a, Bridgette J. Connell^b, Pauline J. Schipper^b, Joost van Dalum^b, Ellen Baeten^c, Dorine van den Blink^c, Andries C. Bloem^c, Monique Nijhuis^b, Annemarie M.J. Wensing^b, Leon W.M.M. Terstappen^a, Markus Beck^{a*}

^a Medical Cell Biophysics, MIRA Institute for Biomedical Technology and Technical Medicine, Faculty of Science and Technology, University of Twente, PO Box 217, Enschede, 7500 AE, The Netherlands

^b University Medical Center Utrecht, Department of Medical Microbiology, Virology, Heidelberglaan 100, 3584CX Utrecht, The Netherlands

^c University Medical Center Utrecht, Laboratory of Translational Immunology, Section Diagnostics, Heidelberglaan 100, 3584CX Utrecht, The Netherlands

*Corresponding Author:

Markus Beck: m.beck@utwente.nl

Table of Contents

Figure S1. Fabrication process of chambers with polysaccharide/Ab layers, by casting.

Figure S2. Schematic representations of fully printed counting chambers including exemplary images of gellan layers and chamber frames

Figure S3. Step-wise polysaccharide material screening process

Figure S4. Fractional release of APC- α CD3 from cast gellan layers stored for different periods of time

Figure S5. Scatter plots and histograms of fluorescence intensities of cells stained with APC- α CD3 and PerCP- α CD4 in counting chambers stored up to 3 months

Figure S6. The stability of APC and PerCP in dry printed gellan layers and the cell count accuracy from printed CD4 counting chambers after 1-week storage subject to different unfavourable conditions

Figure S7. Comparison of CD4 counts of leukocyte-depleted samples, with different leukocyte concentrations from healthy donors, measured using our image cytometry approach and using flow cytometry

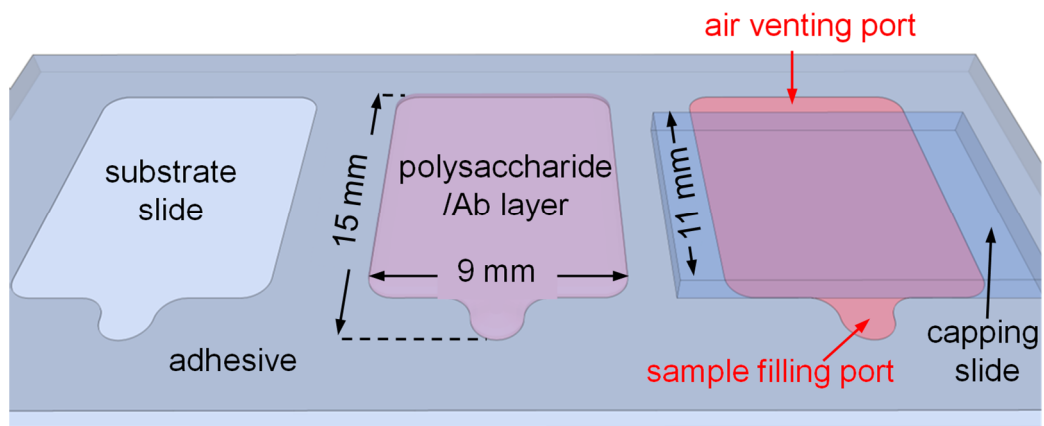


Figure S1. Process flow of chamber fabrication by manual casting, from left to right: empty casting area on a glass substrate, casting area with cast layer and dried cast layer in finished chamber.

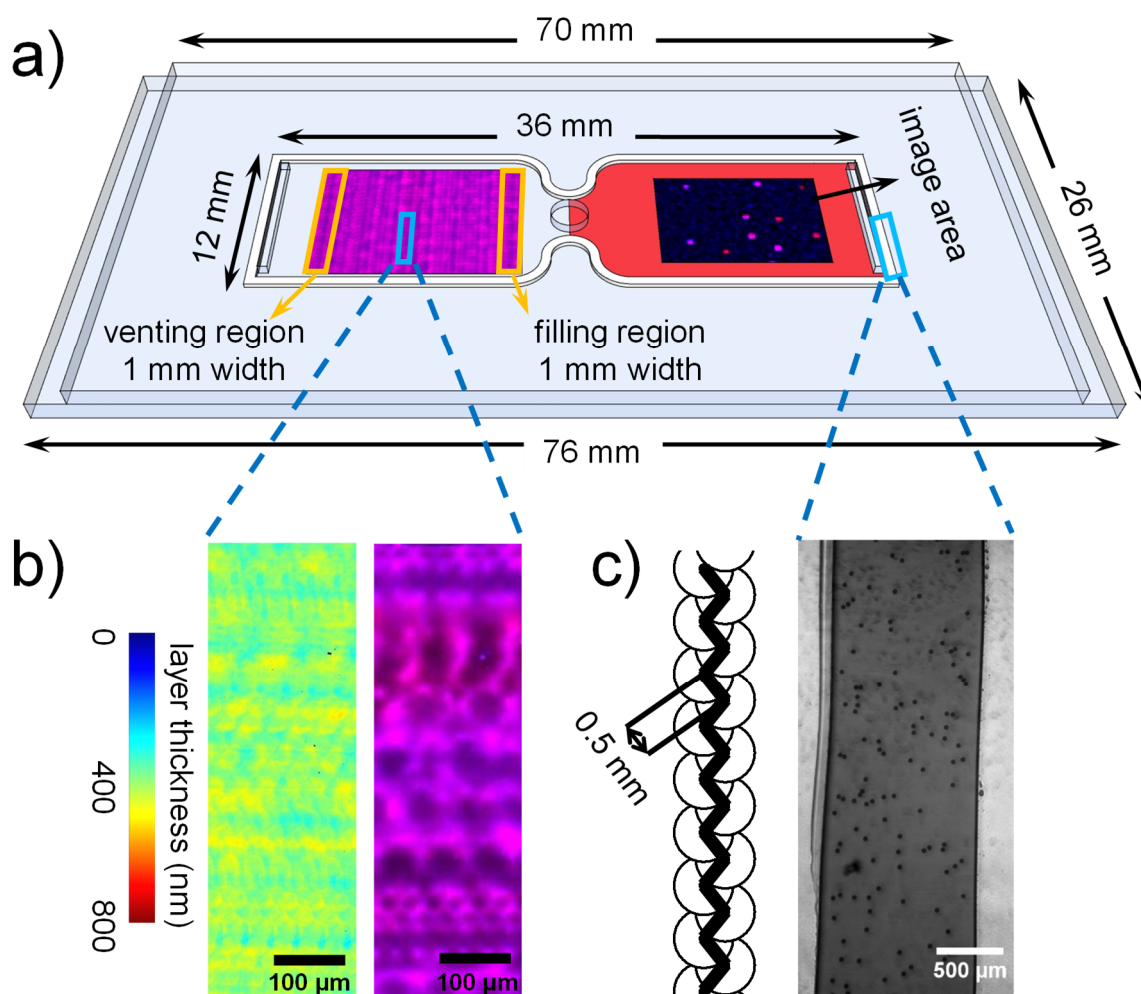


Figure S2. a) Schematic representations of fully printed counting chambers. In the left chamber the fluorescence image of a dry layer, and in the right chamber fluorophore stained cells are shown as overlays of the fluorescence images of both fluorophores (APC and PerCP). b) Left, topographical map of a segment of a printed layer; Right, overlay of fluorescence images (red excitation (APC) and blue excitation (PerCP)) of the same segment. c) Left, print pattern for the deposition of glue/bead suspension for the fabrication of chamber frames (black line represents dispenser path during deposition, circles represent the estimated area covered by the droplet after being deposited on the glass substrate). Right, bright field image of a segment of a cured frame.

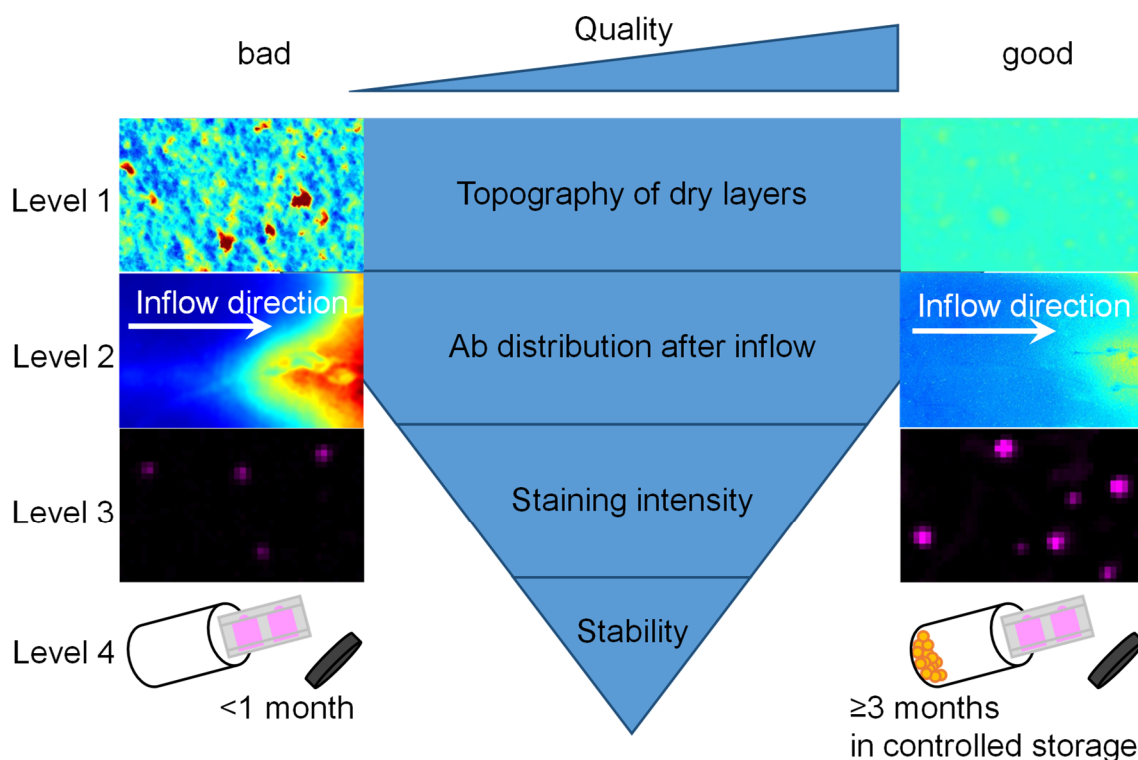


Figure S3. Scheme showing the polysaccharide screening process (center column) with illustrations of bad (left column) and good (right column) matrix materials. Level 1, examples of rough (left) and smooth (right) layers. The color scale ranges from 0 nm (blue) to 100 nm (red). Level 2: images of the concentration gradient of Ab along inflow direction (left to right) in representative chambers. The color scale ranges from blue: low concentration to red: high concentration. The left image is an example of a material causing a steep Ab concentration gradient, while the right image is an example of a material leading to relatively uniform Ab distribution. Level 3: comparison of a material capable of staining cells only weakly (left) with one resulting in well-stained cells (right). Level 4: the stability and functioning of polysaccharide release matrices over time.

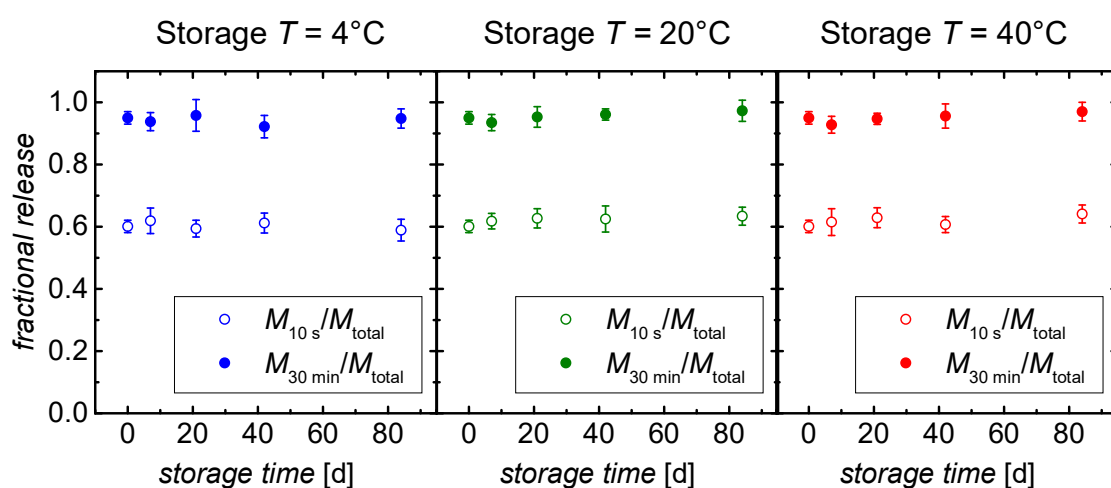


Figure S4. Fractional release of APC- α CD3 after 10 s ($M_{10 s}/M_{total}$, open circles) and after 30 min ($M_{30 min}/M_{total}$, solid circles) incubation from cast gellan layers stored under $\sim 10\%$ RH and at 4°C (blue circles, left), 20°C (green circles, center) and 40°C (red circles, right) over time. Data points represent mean \pm standard deviation ($n = 3$).

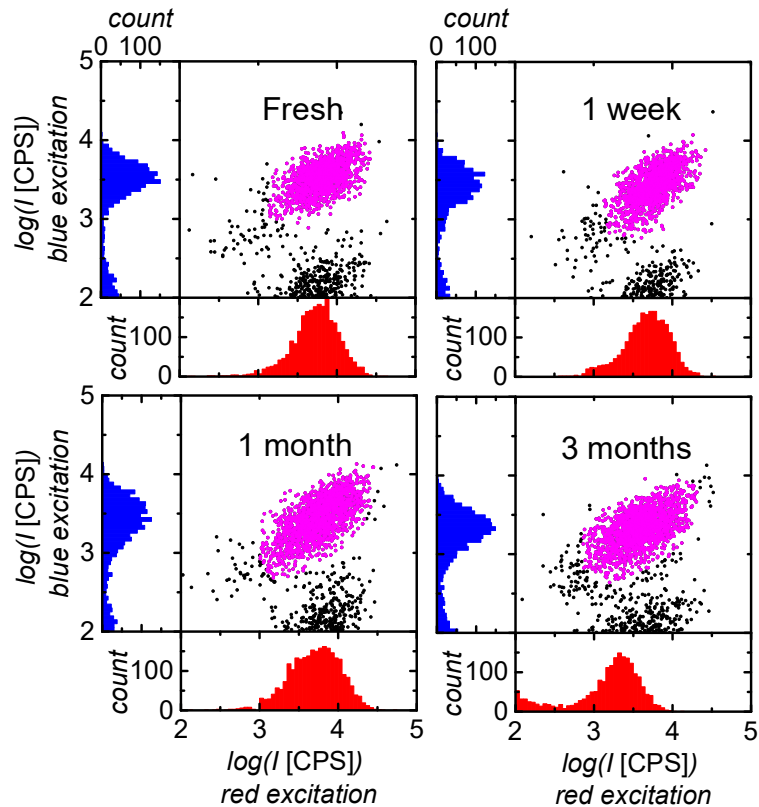


Figure S5. Scatter plots and histograms of fluorescence intensities obtained using our image cytometry method of cells stained with APC- α CD3 (red excitation) and PerCP- α CD4 (blue excitation) in counting chambers stored under 4g condition for different periods of time. The purple circles are the cells belonging to the double positive cell population.

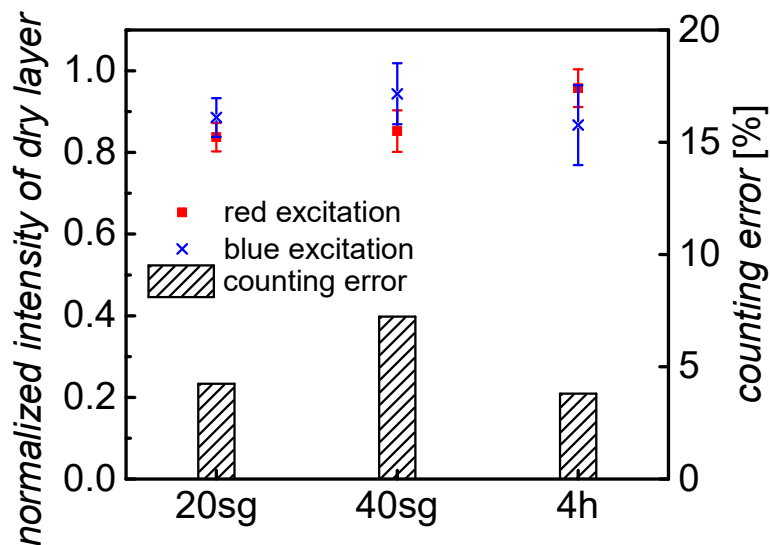


Figure S6. The ratio of fluorescence intensities for both, APC (red squares) and PerCP (blue crosses) readouts of dry printed layers after 1-week storage under less favorable conditions (20sg, silica gel 20°C; 40sg, silica gel 40°C and 4h, high humidity 4°C) and the intensities of the same layers, freshly prepared. Data points represent mean \pm standard deviation ($n = 4$). Average accuracy of the cell count (black columns) obtained from printed CD4 counting chambers, which were stored for 1 week under less favorable conditions that could for example be encountered if cooling is not available continuously or if the seal of a storage container is compromised.

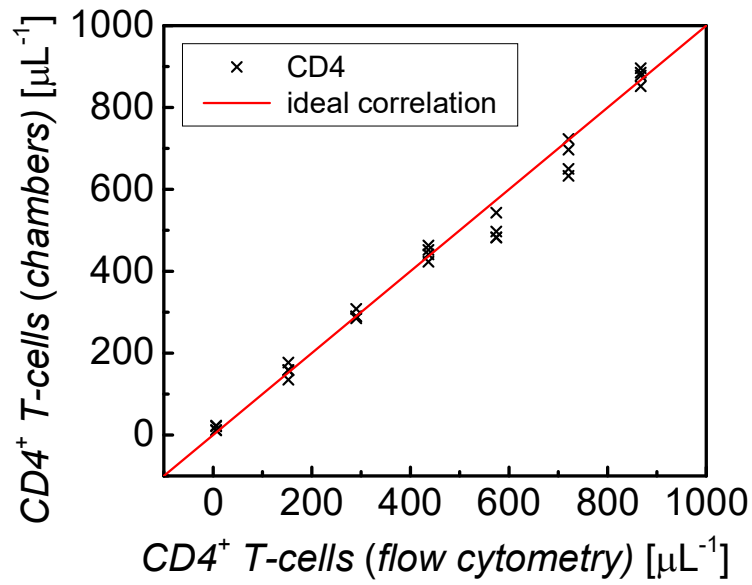


Figure S7. Comparison of CD4 counts (#cells μL^{-1}) of leukocyte-depleted samples, with different leukocyte concentrations from healthy donors measured using our image cytometry approach and using flow cytometry. For each sample with a given leukocyte concentration, 4 separate counting chambers were used (crosses) and 3 separate flow cytometry assays were performed. The individual counts obtained using our image cytometry approach were plotted against each average of the respective flow cytometry results.